

MIT Open Access Articles

Simultaneous Spatial and Temporal Measurements of the Current Distribution in a Miniature Hull Cell

The MIT Faculty has made this article openly available. **Please share** how this access benefits you. Your story matters.

Citation: Chmielowiec, Brian, Truong Cai, and Antoine Allanore. "Simultaneous Spatial and Temporal Measurements of the Current Distribution in a Miniature Hull Cell." *J. Electrochem. Soc.* 163, no. 5 (2016): E142–E146.

As Published: <http://dx.doi.org/10.1149/2.1001605jes>

Publisher: Electrochemical Society

Persistent URL: <http://hdl.handle.net/1721.1/102288>

Version: Final published version: final published article, as it appeared in a journal, conference proceedings, or other formally published context

Terms of Use: Article is made available in accordance with the publisher's policy and may be subject to US copyright law. Please refer to the publisher's site for terms of use.



Massachusetts Institute of Technology



Simultaneous Spatial and Temporal Measurements of the Current Distribution in a Miniature Hull Cell

Brian Chmielowiec,^{a,*} Truong Cai,^b and Antoine Allanore^{a,*,z}

^aDepartment of Materials Science & Engineering, Massachusetts Institute of Technology, Cambridge, Massachusetts 02139, USA

^bDepartment of Chemical Engineering, Massachusetts Institute of Technology, Cambridge, Massachusetts 02139, USA

Experimental validation of the current distribution for actual cell geometries is an important complement to modeling. In this work, the combination of a segmented electrode in a miniaturized Hull Cell with a synchronous monitoring of the current response in each segment is proposed as a novel experimental set-up. The high frequency monitoring of the current response to potential steps is investigated as a mean to access the temporal and spatial evolution of current distribution. The corresponding primary current distribution was measured using a ferricyanide/ferrocyanide alkaline electrolyte, confirming the prediction from Laplace's equation. In addition, the experimental set-up allowed the identification of the transition time from primary to tertiary current distribution regimes.

© The Author(s) 2016. Published by ECS. This is an open access article distributed under the terms of the Creative Commons Attribution 4.0 License (CC BY, <http://creativecommons.org/licenses/by/4.0/>), which permits unrestricted reuse of the work in any medium, provided the original work is properly cited. [DOI: [10.1149/2.1001605jes](https://doi.org/10.1149/2.1001605jes)] All rights reserved.

Manuscript submitted January 7, 2016; revised manuscript received January 19, 2016. Published February 11, 2016.

From a physics standpoint, electrochemical processes (being in fuel-cells, batteries, electrodeposition or electrowinning cells) can be considered as an exchange of electrical and chemical energy, a conversion occurring at the interface between the electrode and the electrolyte. One key objective in the engineering of electrochemical reactors is therefore to achieve a uniform rate of conversion across the electroactive surfaces, i.e. a uniform current density along the electrodes. In actual cells, due to geometrical constraints, non-uniform current distributions develop. The ultimate consequence and importance of this non-uniformity on process performance varies. Limited mass transfer in porous electrodes impregnated with an active material (typically a precious metal catalyst¹) leads to an under-utilization of the electrode. On the other extreme, lithium ion batteries suffering from current inhomogeneity can grow dendrites that ultimately short circuit the positive and negative electrodes, creating dangerous and potentially explosive situations.² Though less acknowledged, non-uniformity in current distribution during electrodeposition in a liquid cathode (including alloying) may result in streamers or composition gradients within the cathode³ which can lead to precipitation of a solid or a short circuit.

The theory of current density distribution has continued to develop since the pioneering work of Kasper, Wagner, Blum, and many others.⁴⁻⁸

Three types of contributions are typically taken into account to evaluate the actual current distribution in an electrochemical reactor. The first contribution, leading to the primary current distribution, is due to resistance to current flow inherited from the finite conductivity of the electrolyte. This primary current distribution is entirely dictated by the conductivity of the electrolyte and the geometry of the electrodes and the cell. The second contribution is inherited from resistance to current flow due to the presence of faradaic reactions at the electrodes and leads to the secondary current distribution. The electrochemical reaction kinetics that link the electrode potential to the faradaic current, e.g. as described by Butler-Volmer equations, are taken into account in addition to the ohmic, primary contribution. The third contribution is related to mass transfer phenomena, which dictate concentration gradients that can affect the ability for the faradaic reaction to be sustained. Integrating ohmic, kinetic and mass transfer phenomena to evaluate the current distribution leads to the tertiary current distribution. The combined choice of the electrolyte, the electrochemical reactions, the cell geometry, and the range of current density investigated dictates the relative importance of each contribution to the current distribution.

The seminal paper⁹ by Newman and Tobias on current distribution within porous electrodes championed the calculation of the tertiary distribution. Thanks to the development of powerful computational methods, this field is nowadays typically treated in a theoretical manner, with commercial packages that allow one to evaluate primary, secondary, and even tertiary current distributions reasonably quickly. Landolt, West, and Matlosz calculated the primary current distribution for the Hull Cell.¹⁰ Lavelaine de Maubeuge determined the optimal geometry of electrochemical cells for a targeted, arbitrary current distribution.¹¹

To validate this theoretical framework, a couple of experimental techniques have been developed, particularly in the context of metal electrodeposition. Alkire, Landolt, and West pioneered measurements of current distributions with resistive electrodes.¹²⁻¹⁵ Fukunaka successfully employed holographic interferometry to study the diffusion boundary layer in aqueous cells undergoing natural convection with a uniform current distribution and correlated this to theoretical predictions.^{16,17} Landolt and Matlosz extended treatment of the classic Hull Cell to study secondary current distribution effects.¹⁸ Most of the reported experimental studies do not address the issue of short time current transients (less than 100 ms), monitored simultaneously across a given electrode surface. Such an issue is of interest when knowledge of the rate of progression of surface or bulk diffusion layers toward confined locations is desired. In other words, how and when does a given location along a surface where electrochemical reactions are conducted become electrochemically active under different current distribution regimes?

Previous efforts at monitoring multiple electrodes have been limited to low currents (pico to nano amp levels), usually in a multiplex mode, thereby not providing a truly synchronous monitoring of the current at each electrode.¹⁹⁻²² The fuel cell community utilizes segmented electrodes, and operates with high currents.²³ Interestingly, there are limited efforts to simultaneously monitor the current density at multiple electrodes for a given cell geometry, in particular at a scale representative of hydrodynamic phenomena. In addition, most studies are conducted at constant total current, and not constant cathode potential, thereby limiting the ability to control the selectivity of the electrochemical reactions.

In this paper we document the first (to our knowledge) experimental apparatus that allows for the simultaneous measurement of current flowing through eight separate working electrodes with high temporal resolution, down to 10 μ s. This resolution allows to monitor in-operando the primary current distribution without interferences from external probes, and to identify the critical time when other types of phenomena start to affect the current flow. The results open the path toward investigating the impact of surface inhomogeneity - being chemical or physical - on current transients. Ultimately, such

*Electrochemical Society Student Member.

**Electrochemical Society Member.

^zE-mail: allanore@mit.edu

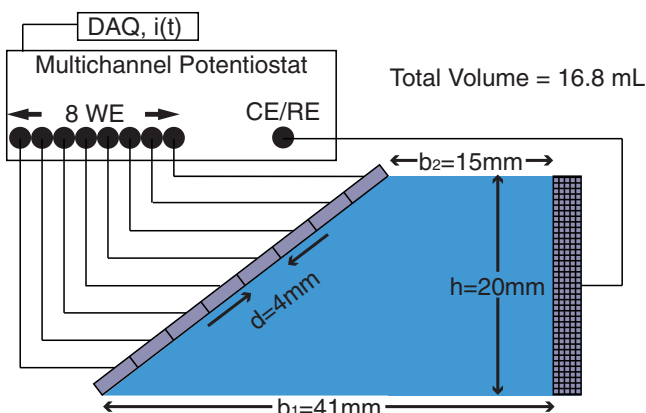


Figure 1. Schematic of cell and measurement apparatus. The minimum and maximum working-counter electrode distances are 15 mm and 41 mm, respectively. The analog outputs of the potentiostat are recorded as digital signals using synchronous data acquisition units. An example of the potential waveform applied to all eight working electrodes simultaneously is presented on the right.

an approach allows the experimentalist to evaluate how an electrochemical cell accommodates an inhomogeneous primary current distribution.

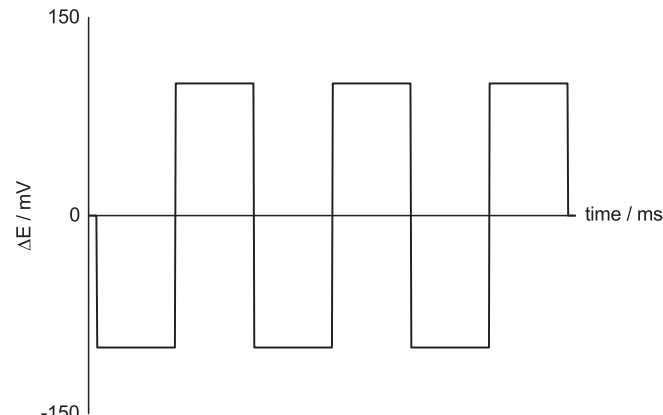
Experimental

Cell materials.—The cell was constructed from acrylic, selected for its high chemical resistance to alkaline aqueous solutions and to allow visual confirmation that the entire Hull Cell was filled with electrolyte. The cell walls were laser cut to give a cell volume of 16.8 mL. The critical dimensions of the cell are given in Figure 1.

Electrolyte.—To enhance the ability to probe the primary current distribution, a reaction with facile kinetics, the ferricyanide/ferrocyanide redox couple was selected. The solution was obtained by dissolving powders of potassium hexacyanoferrate (III) and potassium hexacyanoferrate (II) trihydrate (Alfa Aesar, 99+%) and pellets of potassium hydroxide into an appropriate amount of ASTM-II grade water to give concentrations of 10.0 mM of electroactive species, and 100.0 mM or 1000.0 mM of supporting electrolyte. Given these compositions, the chosen cell and the electrodes geometry, the associated Wagner number for the cell under study was around 10^{-5} – 10^{-3} ($\ll 1$), validating the assumption that the secondary current distribution is nearly the same as the primary current distribution.

Electrodes.—Each of the eight working electrodes were water-jet cut from the same 2 mm thick nickel plate (Alfa Aesar, 99.99%) to ensure minimal compositional differences. The dimensions of each electrode were 30 mm \times 4 mm \times 2 mm. A 10 cm long nickel wire was soldered to the back of each electrode prior to the casting of the electrodes in epoxy, with electrical tape insulating the adjacent surfaces from each other. After curing, this eight electrode array was polished sequentially with 180, 320, 600, 1200, and 2000 grit Silicon Carbide sandpaper before polishing with 1 μm and 0.3 μm alumina paste (Bueeler). Finally, electrochemical pre-treatment was conducted using the electrolyte without ferri/ferrocyanide, evolving hydrogen as prescribed in previous studies.²⁴ To ensure a large surface area counter electrode, a 50 mesh nickel gauze with wire diameter of 50 μm (Alfa Aesar) was used, with dimensions of 20 mm \times 30 mm.

Electrochemical measurements.—The current at each working electrode was synchronously measured using a CHI1040C multichannel potentiostat. The nickel mesh counter electrode was shared by all of the working electrodes. Figure 1 depicts schematically the recording circuit. Each working electrode was held at the same potential versus the counter electrode, and no reference electrode was used. Chronoamperometry measurements were performed during three (3) anodic/cathodic (double) potential steps of $\Delta E = \pm 100$ mV or



± 10 mV for the low and high supporting electrolyte concentrations, respectively. These potentials were chosen to give large current responses without exceeding the compliance current of the potentiostat at ± 10 mA per channel. The duration of the steps was fixed during each experiment, but was varied across experiments. To improve the temporal resolution of the measurement, two data acquisition units (DAQ, Data Translation 9837B) were used to monitor the current response of each electrode synchronously at 100 kHz/electrode via the analog output of the potentiostat. To benefit from this enhanced sampling rate, it proved imperative to turn off any filtering from the potentiostat. The acquisition units were manually calibrated in order to convert the measured voltages into currents. Linear calibration resulted in excellent fits with R^2 values > 0.9999 .

Simulation.—The steady-state primary current distribution for the cell used in this study was simulated using the Electric Currents Physics in the AC/DC Module of Comsol Multiphysics, version 4.2. All dimensions were identical to those belonging to the experimental cell. The electrolyte conductivity was taken to be 20 or 2 $\text{S}\cdot\text{m}^{-1}$, the conductivity of 1 M or 0.1 M potassium hydroxide solutions, respectively.²⁵ The Electric Currents Physics module offers to solve Laplace's Equation (Eq. 1a) within the electrolyte, with appropriate constant potential boundary conditions at the counter electrode (Eq. 1b) and working electrodes (Eq. 1c), where φ is the potential:

$$\nabla^2 \varphi = 0 \quad [1a]$$

$$\varphi(x = x_{CE}) = 0 \quad [1b]$$

$$\varphi(x = x_{WE}) = \Delta E \quad [1c]$$

Simulation parameters.—Values of the mesh size did not impact the predicted currents by more than 0.2%. Running the simulation varying ΔE or the electrolyte conductivity confirmed a relative variation in current density entirely governed by geometry. Interested only in relative differences across the working electrodes, the normalization factor was chosen to be the total current flowing through the cell.

Cottrell-type diffusion model.—In the selected conditions, diffusion of the reactants and products of the sole reaction foreseen on the working electrodes is likely to govern the current density variation with time at each electrode after charging of the electrochemical double layer is complete, thus entering the realm of a tertiary current distribution. Therefore, a Cottrell-like model²⁶ that takes into account the square root of time dependence of the current density has been adopted. The analytical model is given in Eq. 2 whose symbols are

Table I. Parameters Used for Diffusion Model.

n	1	# of electrons exchanged
F	96485	Faraday's Constant in Cmol ⁻¹
D	6 to 7×10^{-10}	Diffusivity of K ₄ Fe(CN) ₆ and K ₃ Fe(CN) ₆ ²⁹ in m ² s ⁻¹
C _{bulk}	10	Bulk Concentration of K ₄ Fe(CN) ₆ and K ₃ Fe(CN) ₆ in mM

detailed in Table I:

$$j_k = \frac{nFD^{\frac{1}{2}}(C_{bulk} - C_k)}{\pi^{1/2}(t - t_k)^{1/2}}, \quad k = 1, 2, \dots, 8 \quad [2]$$

C_k is the surface concentration of the electroactive species, presumably following the Nernst equation. t_k is the time offset (the pulse is not applied at t = 0), and k is the electrode number. The Scilab (Scilab Entreprise) function, *lsqrsolve*, was utilized to fit the above nonlinear model to the data. Performing a nonlinear fit is complementary to the traditional approach of changing variables to generate a linear plot (e.g. linear regression of j vs t^{-1/2}), but avoids the issue of underweighting certain data points that tend to cluster together upon transformation of the independent variable. The time range over which the model was deemed valid was determined as the range in which the figure of merit, FOM (an objective function) was sufficiently small:

$$FOM = \frac{1}{N} \sum_{n=1}^N \frac{(y_n - f_n)^2}{\left[\frac{1}{2} (y_n + f_n) \right]^2} \leq 10^{-5} \quad [3]$$

Where N is the number samples involved in the fit, y_n is the current density for sample n, and f_n is the value of the fitted function at sample n.

Results

Current density.—The current response of the cell recorded during a sequence of cathodic and anodic steps is shown in Figure 2. Three sequences are typically recorded. A reproducible response develops after the first anodic step completes. The peaks are not observed in the absence of ferricyanide and ferrocyanide. The electrode numbers represent the distance of each working electrode from the counter electrode, with #1 being closest, and #8 being furthest away. Due to the large difference in current spanned across the eight electrodes (almost two orders of magnitude), it proved necessary to record the more recessed channels with a more sensitive current range to reduce noise. The minimum value of the current range was dictated by the initial current response to the potential steps. In order to observe a current peak and not a current plateau, the selected current range needed to be sufficiently high to avoid the so-called galvanometric constraints

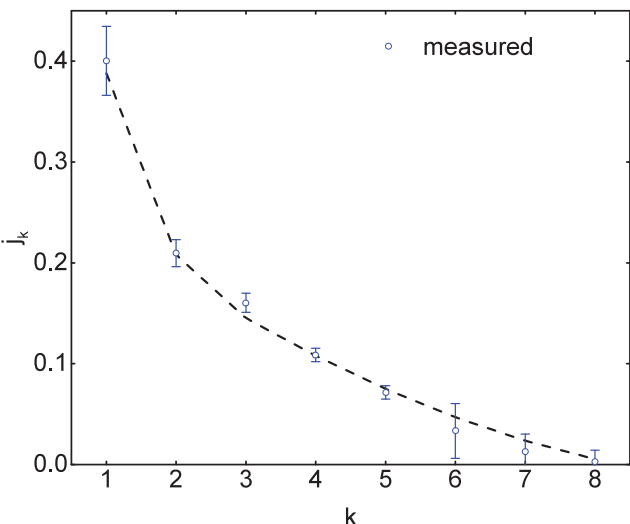


Figure 3. Measured current density on each electrode k, reported as the normalized peak current recorded after each potential step (Equation 4). Error bars indicate ± 2 standard deviations from the mean. The dashed line shows the prediction from primary current distribution calculation.

discussed by Wein.²⁷ For most measurements a range of 10 mA and 1 mA was used respectively for the four electrodes closest to the counter and the four electrodes furthest away. Figure 3 shows the peak current recorded at each electrode k in response to each of the applied pulses, normalized by the total current as expressed in Eq. 4.

$$\bar{j}_k = \frac{i_k(t_{peak}) / A_k}{\sum_{e=1}^8 i_e(t_{peak}) / A_e} \quad [4]$$

A Scilab script was written to find t_{peak} corresponding to the peak current recorded on electrode 1. Since care was taken to obtain electrodes with the same geometric surface area, the normalized current density, \bar{j}_k is equivalent to the normalized current density calculated in the simulation. In Figure 3, the peak current density is reported versus electrode number as the x-axis, equivalent to distance from the counter electrode. These measurements were repeated multiple times and for different pulse sizes, durations, and supporting electrolyte conductivity. A cumulative plot of all these measurements is presented in Figure 4, where the diagonal represents the primary current density distribution predicted by the simulation. Table II reports the range of experimental conditions gathered in Figure 4, for which good agreement exists between experiment and simulation.

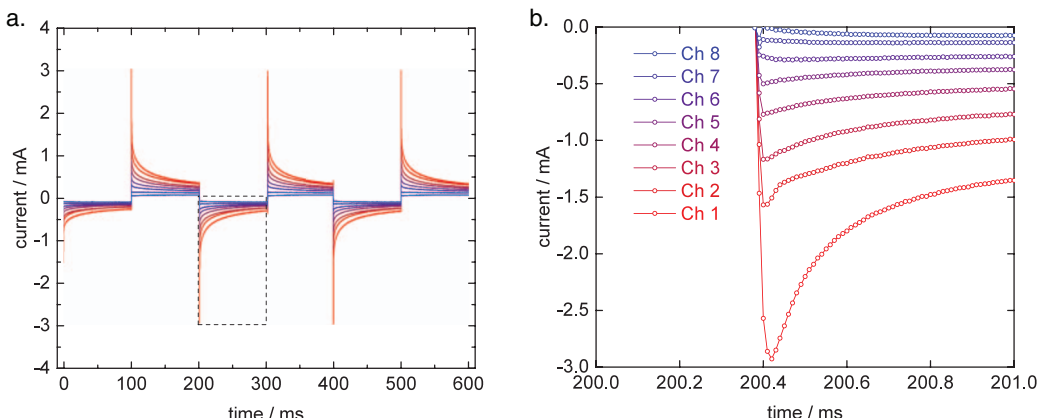


Figure 2. (a) Current response to the potential waveform. (b) Current response immediately after the third potential step. (potential steps of ± 100 mV and pulse duration of 100 ms).

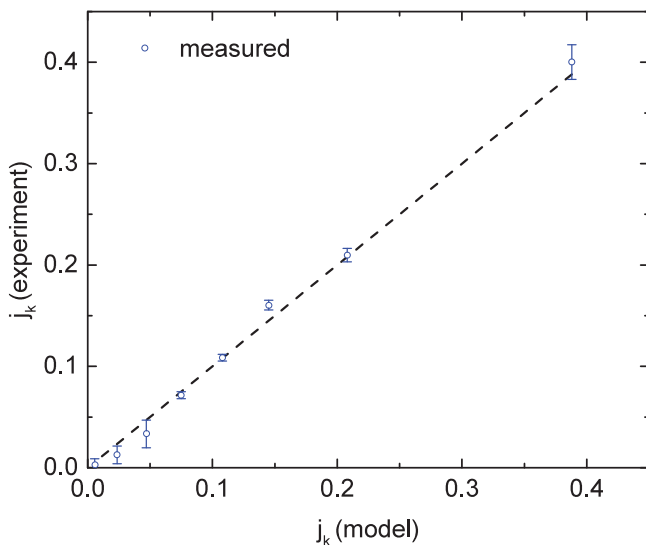


Figure 4. Cumulative comparison between measured and calculated current distributions. Measured data include peaks recorded for all the steps and for multiple step sizes, step durations, and supporting electrolyte compositions (see Table II for the list of conditions included). Error bars indicate ± 2 standard deviations from the mean. The dashed line shows the prediction from the primary current distribution calculation.

Long term current behavior.—In addition to studying the current response immediately after the pulse, the long-term (>20 ms) decay of current was recorded, as reported in Figure 5. After sufficiently long times it is anticipated that diffusion limits the mass transport to the electrode surface and thus the current. The current in Figure 5 has therefore been fitted to a Cottrell-like model (Eq. 2), a fit that proved valid for a time always greater than 30 ms, with no systematic variation with the electrode number or position.

Discussion

It proves possible, via high acquisition rate (100 kHz per electrode) to detect a peak current for segmented electrodes along the confined side of a Hull cell, in response to a step in the cell voltage. This peak is attributed to the primary current based on the exceptional agreement between the simulation and our results (Fig. 4). Sampling at a higher rate of acquisition may have diminishing returns, as one must consider the rise time of the potentiostat circuitry, which for the present equipment, is 2 μ s. Stable electrical responses can only be expected after two to three time constants of the circuitry. We found that the timing of the peak current was very repeatable, between 40 and 50 μ s (4 to 5 samples) after the application of the potential step. It also proved independent of the step size within the investigated range. This feature indicates that the measurement does not interfere with the rise time of the analog to digital converters of the data acquisition systems. The lack of discernable peaks in the absence of ferricyanide and ferrocyanide indicates that hydrogen evolution has negligible contribution to the overall current over the chosen potential window ($|\Delta E| < \pm 300$ mV). As expected, the current is highest for electrode 1 which experiences the lowest electrolyte resistance, while the smallest current flows through electrode 8 for similar reasons. Figure 4 shows that the recorded data match remarkably well with the

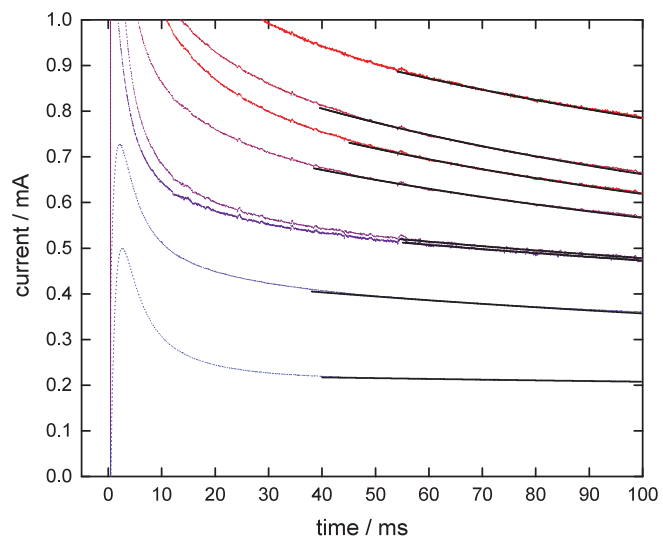


Figure 5. Long-term current transient (color legend as in Figure 2). The thick black line represents the current as fitted to Equation 2 using the figure of merit given in Equation 3. The beginning of the black line establishes the time for which the current becomes controlled by diffusion.

primary current distribution simulations. For step durations greater than 10 ms, the predicted values fall within the experimental error for all the electrodes except electrode 3, which consistently records a current higher than the predictions. A slightly smaller internal resistance in the potentiostat for this channel would account for more negative (resp. positive) potentials at the electrode surface during the negative (resp. positive) potential steps.

Thanks to the identification of an electrical event that is a signature of the primary current distribution, the proposed method also allows to identify the time-scale at which other type of current distributions become important. In the present case, a contribution of bulk diffusion has been demonstrated as determined by a non-linear analytical fit. Such a numerical method is preferred to a linearization of the current versus time because of the short duration of the steps (100 ms) and the relatively low currents. Close to the end of the step, the magnitude of $t^{-1/2}$ becomes quite small such that when computing the derivative numerically, the denominator $(t_{i+1}^{-1/2} - t_i^{-1/2})$ inflates the derivative and leads to high levels of noise. Analysis of Figure 5 shows that the current indeed follows semi-infinite linear diffusion from a planar electrode, though only 30 to 40 ms after the onset of the potential step. Several factors may affect the time needed for diffusion to control the current. At the earliest times, double layer charging results in an exponentially decaying current. While this current is initially quite large ($\Delta E/R \sim 1$ to 10 mA for the present geometry) it is expected to decay rapidly ($3RC \sim 7$ ms for the most isolated electrode assuming the double layer capacitance C to be $10\text{--}20 \mu\text{F/cm}^2$). Another cause for the delay in observing diffusion controlled current may be the non-negligible ohmic-drop to the counter electrode, due to the absence of a reference electrode. Dhillon and Kant²⁸ for example reported via calculation that resistive effects are non-negligible roughly during the first tens of milliseconds of a chronoamperometry experiment, similar to our finding. The present work aimed to minimize the effects of the counter electrode on the current distribution by utilizing a high surface area mesh to reduce activation overpotential and positioned the electrode sufficiently far away from the working electrodes to ensure a uniform current distribution on the counter electrode as predicted by the simulation. The superior temporal resolution of the present technique provides ample data points to analyze the evolution of the ohmic drop and its effect on the current distribution. Such study may become necessary in the future for researchers interested in better describing the early (<40 ms) time scale results and refine models.

The demonstrated ability to decipher with an enhanced spatial and temporal resolution the nature of the phenomena that govern the

Table II. Experimental Conditions Represented in Figure 4.

Supporting Electrolyte Concentration (mM)	Potential Step Amplitude (mV)	Pulse Length (ms)
100	$\pm 50, 100, 250$	100
1000	$\pm 10, 50$	100

current flowing on a given electrode surface at a fix electrical potential, may be of interest to electrochemical engineers in general. In particular being able to experimentally identify simultaneously across a given surface at which timescale each phenomenon becomes important is a novel feature. While the results presented in this work are for the limiting case of $Wa \rightarrow 0$, the approach can and should be extended to systems whose secondary current distributions diverge from their primary current distributions, such as frequently observed in metal electrodeposition. For example, one possible extension of our approach could be to consider perturbing the electrolyte present in front of one region of the cell (e.g. in front of electrode 8, the most recessed) by injecting a more electropositive and active species, in order to assess how fast and for how long the current would be ‘pulled’ toward this un-favored region from a primary current standpoint. This would be the chemical equivalent of having an additional counter electrode positioned nearby whose potential slowly varies with time. Such a technique could be of interest in understanding transient inhomogeneity in alloy deposition formed at constant potential.

Conclusions

The simultaneous, high frequency monitoring of the current in a segmented electrode operated potentiostatically demonstrated the ability to determine both the primary and tertiary current distribution in-operando. Within the first tens of microseconds after the step in the cell voltage, the system is found to obey the primary current distribution. Transition to a current density distribution controlled by diffusive flux of the analyte to the working electrode was determined via nonlinear fitting of the recorded current to a prescribed accuracy using a normalized residual.

Acknowledgments

This research work was partially supported by the Office of Naval Research (contract #N00014-12-1-0521) and the National Science

Foundation (award #1449644). The authors acknowledge valuable discussions with David Bono regarding the electrical engineering aspects of the work.

References

1. K. Mund and F. von Sturm, *Electrochim. Acta*, **20**, 463 (1975).
2. S. Liu, N. Imanishi, T. Zhang, A. Hirano, Y. Takeda, O. Yamamoto, and J. Yang, *J. Electrochem. Soc.*, **157**, A1092 (2010).
3. W. Pongsaksawad, A. C. Powell, and D. Dussault, *J. Electrochem. Soc.*, **154**, F122 (2007).
4. C. Kasper, *ECS Trans.*, **77**, 353 (1940).
5. C. Kasper, *ECS Trans.*, **78**, 147 (1940).
6. C. Wagner, *J. Electrochem. Soc.*, **98**, 116 (1951).
7. C. Wagner, *J. Electrochem. Soc.*, **107**, 445 (1960).
8. H. E. Haring and W. Blum, *Trans. Am. Electrochem. Soc.*, **43**, 365 (1923).
9. J. S. Newman and C. W. Tobias, *J. Electrochem. Soc.*, **109**, 1183 (1962).
10. A. C. West, M. Matlosz, and D. Landolt, *J. Appl. Electrochem.*, **22**, 301 (1992).
11. H. Lavelaine de Maubeuge, *J. Electrochem. Soc.*, **149**, C413 (2002).
12. R. Alkire, *J. Electrochem. Soc.*, **118**, 1935 (1971).
13. R. C. Alkire and A. Tvarusko, *J. Electrochem. Soc.*, **119**, 340 (1972).
14. M. Matlosz, P. H. Vallotton, A. C. West, and D. Landolt, *J. Electrochem. Soc.*, **139**, 752 (1992).
15. P. H. Vallotton, M. Matlosz, and D. Landolt, *J. Appl. Electrochem.*, **23**, 927 (1993).
16. Y. Fukunaka, T. Minegishi, N. Nishioka, and Y. Kondo, *J. Electrochem. Soc.*, **128**, 1274 (1981).
17. S. Kawai, Y. Fukunaka, and S. Kida, *J. Electrochem. Soc.*, **155**, F75 (2008).
18. M. Matlosz, C. Creton, C. Clerc, and D. Landolt, *J. Electrochem. Soc.*, **134**, 3015 (1987).
19. D. De Venuto, M. D. Torre, C. Boero, S. Carrara, and G. De Micheli, *IEEE Sensors*, **15**, 1572 (2010).
20. N. M. Contento and P. W. Bohn, *Microfluid. Nanofluidics*, **18**, 131 (2014).
21. H.-J. Yee, J.-K. Park, and S.-T. Kim, *Sensors Actuators B*, **34**, 490 (1996).
22. J. Yao, X. A. Liu, and K. D. Gillis, *Anal. Methods*, **7**, 5760 (2015).
23. M. M. Mench, C. Y. Wang, and M. Ishikawa, *J. Electrochem. Soc.*, **150**, 1052 (2003).
24. D. A. Szanto, S. Cleghorn, C. Ponce-de-Leon, and F. C. Walsh, *AICHE J.*, **54**, 802 (2008).
25. R. C. Weast, *CRC Handbook of Chemistry and Physics*, 70th Edition, p. D, (1989).
26. O. Kozaderov and A. Vvedenskii, *Russ. J. Electrochem.*, **37**, 798 (2001).
27. O. Wein and V. V. Tovchigrechko, *J. Appl. Electrochem.*, **41**, 1065 (2011).
28. S. Dhillon and R. Kant, *Electrochim. Acta*, **129**, 245 (2014).
29. A. J. Arvfa, S. L. Marchiano, and J. J. Podest, *Electrochim. Acta*, **12**, 259 (1967).